ACS APPLIED MATERIALS & INTERFACES

RESEARCH ARTICLE

www.acsami.org

Controllable Growth of Highly Ordered ZnO Nanorod Arrays via Inverted Self-Assembled Monolayer Template

J. J. Dong,[†] X. W. Zhang,[*,†] Z. G. Yin,[†] S. G. Zhang,[†] J. X. Wang,[‡] H. R. Tan,[†] Y. Gao,[†] F. T. Si,[†] and H. L. Gao[†]

[†]Key Lab of Semiconductor Materials Science, Institute of Semiconductors, Chinese Academy of Sciences, Beijing, 100083, P. R. China, and

[‡]Semiconductor Lighting Technology R&D Center, Institute of Semiconductors, Chinese Academy of Sciences, Beijing 100083, P. R. China

Supporting Information

ABSTRACT: This article presents a facile and effective approach to the controllable growth of highly ordered and vertically aligned ZnO nanorod arrays on the GaN substrate via a hydrothermal route by using the TiO_2 ring template deriving from the polystyrene microsphere self-assembled monolayer. The size of TiO_2 ring template can be flexibly tuned from 50 to 400 nm for the 500 nm polystyrene microspheres by varying the time of reactive ion etching and the concentration of TiO_2 sol. As a result, the diameter of the individual ZnO nanorods can be potentially tuned over a wide range. The combination of several characterization techniques has demonstrated that the ordered ZnO nanorods are highly uniform in diameter and height with perfect alignment and are epitaxially grown along [0001] direction. This work provides a novel and accessible route to prepare oriented and aligned ZnO nanorod arrays with high crystalline quality.

KEYWORDS: Zinc oxide nanorods, Hydrothermal synthesis, Inverted self-assembled monolayer, Reactive ion etching, Epitaxial growth

1. INTRODUCTION

Wurtzite ZnO is considered the most promising material for short wavelength optoelectronic devices because of its large band gap of 3.36 eV, high exciton binding energy of 60 meV, and high mechanical and thermal stabilities at room temperature. ZnO nanostructures such as nanowires, nanorods, nanorings and nanotubes, have attracted extensive attention over the past few years, because of their unique electrical and optical properties.[1−3] In particular, patterned and aligned one-dimensional (1D) ZnO nanostructure arrays, which can bring about improved performance of multifunctional devices and systems, are the most attractive. Dimension adjustable, highly oriented, periodic ZnO nanorod/nanowire arrays are highly desirable for the realization of advanced photonic optical devices.[4−7] Traditionally, the fabrication of patterned and aligned 1D ZnO nanostructure arrays can be achieved via vapor−liquid−solid (VSL) growth on the patterned catalyst/seed sites created by electron-beam lithography (EBL),[8] laser interference lithography (LIL),[9] or nanoimprint lithography (NIL).[10,11] However, the temperature for VSL method is too high for direct application on various substrates. Furthermore, it may also have the risk of introducing catalyst residual atoms into ZnO. Compared with the conventional VSL method, hydrothermal growth is a low-temperature, catalyst-free process with no limitation of substrates.[5,12−16] Actually, the patterned and aligned 1D ZnO nanostructure arrays have been synthesized with various patterning technologies, such as EBL, LIL, NIL and self-assembled nanosphere lithography (NSL). Among them, NSL has been proven to be a simple and cost-effective technique for the patterning of nanostructure arrays with long-range periodicity in a large scale.[16−18] It employs self-assembled monolayer (SAM) colloidal crystals as the mask to create a patterned seed layer or substrate to guide the growth of nanostructures. For the hydrothermal growth of 1D ZnO nanostructures on patterned substrate created by NSL, however, the resulting ZnO nanostructures are usually not an individual nanorod/nanowire on each growth site, but randomly distributed and of poor crystallization,[19,20] which largely limits their application in high performance optoelectronic devices.

In this article, a facile and effective approach to the controllable growth of highly ordered and vertically aligned ZnO nanorod arrays on the GaN substrate by inverted SAM template via a hydrothermal route is reported. For the preparation of the patterned GaN substrate, TiO_2 sol was used to replicate the SAM of polystyrene (PS) microspheres, and the TiO_2 ring template was obtained by extracting the PS microspheres with toluene. Here, TiO_2 was used as a model material, because it possesses good photocatalytic, optical, gas-sensing, and electronic properties. ZnO grows from the unmasked area of the GaN substrate, and the coalescence of multiple ZnO nanorods to a thicker nanorod from single growth site can be realized at the appropriate solution concentration and reaction temperature. The size of TiO_2 ring template can be tuned flexibly by varying the time of reactive ion etching (RIE) and the concentration of TiO_2 sol. Consequently, the diameter of the individual ZnO nanorods can be potentially tuned over a wide range. The ordered ZnO nanorods are highly uniform in diameter and height with perfect alignment and are epitaxially grown along [0001] direction. This work provides a novel and accessible route to prepare oriented and aligned ZnO nanorod arrays with high crystalline quality.

Received: August 2, 2011
Accepted: October 3, 2011
Published: October 03, 2011

2. EXPERIMENTAL SECTION

A 2.5 wt % suspension of monodispersed PS microsphere with a diameter of 500 nm was purchased from Alfa Aesar and used as received. The PS microsphere monolayers were first self-assembled on a Si (100) wafer by dip-coating, and then transferred to the GaN substrates. Prior to dip-coating, the Si (100) wafer was immersed in piranha solution (98% H_2SO_4:37% H_2O_2 = 7:3) for 3 h to achieve a completely hydrophilic surface. The dipping speed was kept at a constant of 0.5 mm/s. During the transfer process, once the PS coated Si wafer contacted the surface of still water, the PS microsphere SAM was observed to depart from the Si wafer and suspend on the water surface, then it was lifted up with the GaN substrates quickly. After being dried in air, the PS microsphere SAM was obtained. For the preparation of TiO_2 ring template, the TiO_2 sol was first synthesized from the precursors of titanium(IV) isopropoxide, 2-methoxyethanol and ethanolamine according to ref.[21] Then, the TiO_2 sol diluted by isopropanol was applied on the PS microsphere SAM by spin-coating with a speed of 4000 r/min for 80 s. After staying for 3 h for solidification of the TiO_2 sol, the PS microspheres were completely removed by sonication in toluene for 30 min, and the TiO_2 ring arrays were obtained. To adjust the inner diameter of TiO_2 rings, the PS microsphere SAM suffered oxygen RIE with an Alcatel 601E system at 20 mTorr and 100 W. By varying the etching time and the concentration of TiO_2 sol, the inner diameter of the TiO_2 ring template can be tuned conveniently. The isotropic plasma etching of the PS microspheres was performed by a homemade system.

To grow the patterned ZnO nanorod arrays, the GaN substrate with the TiO_2 ring template was fixed up-side down in the reaction vessel filled with aqueous solution of 0.05 M $Zn(NO_3)_2 \cdot 6H_2O$ (99.5% purity, Aldrich) and hexamethylenetetraammine (HMTA) (99.5% purity, Aldrich). Then, the reaction vessel was sealed and kept at a constant temperature for a certain time. Finally, the sample was taken out, rinsed in deionized water and dried in air for characterization.

Surface morphologies and microstructures of the samples were characterized by atomic force microscopy (AFM, NT-MDT Solver P47) using a semicontact mode, field-emission scanning electron microscopy (SEM, Hitachi FE-S4800). The crystal structure identification of the patterned ZnO nanorod arrays was performed by X-ray diffraction (XRD) in a θ-2θ configuration using a Rigaku Dmax 2500 diffractometer with a Cu K_α X-ray source, and the rocking curves and phi-scan of XRD were measured using a Rigaku TTR III diffractometer. Raman scattering measurements were carried out at room temperature with a Horiba LabRAM HR800 spectrometer using the 514 nm excitation lines from an Ar ion laser.

3. RESULTS AND DISCUSSION

The fabrication sequence of ZnO nanorod arrays is schematically illustrated in Figure 1. First, the highly ordered monolayer of PS microspheres was self-assembled on the GaN substrate by dip-coating combined with a transfer process. Then, oxygen RIE was introduced to etch the PS microspheres to the desirable size. Next, TiO_2 sol was prepared and applied on the GaN substrate with the ordered monolayer of PS microspheres by spin-coating. After solidification of the TiO_2 sol, the PS microspheres were removed by sonication in toluene, and the nanoporous TiO_2 ring template was obtained. Finally, a low temperature hydrothermal method was used to achieve the patterned and aligned growth of ZnO nanorod arrays on the patterned GaN substrate.

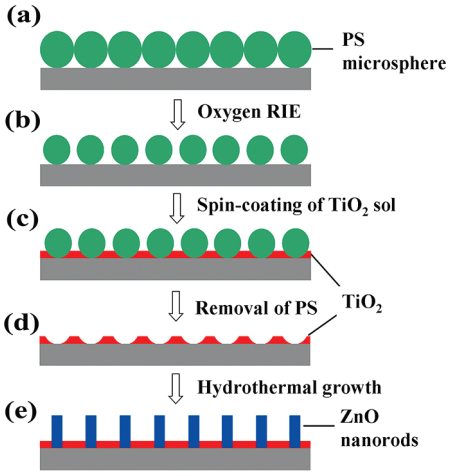

Figure 1. Schematic illustration of the fabrication process of patterned ZnO nanorod arrays. (a) The highly ordered monolayer of PS microspheres was self-assembled on the GaN substrate by dip-coating combined with a transfer process. (b) Oxygen RIE was introduced to etch the PS microspheres to the desirable size. (c) TiO_2 sol was prepared and applied on the GaN substrate with the ordered monolayer of PS microspheres by spin-coating. (d) After solidification of the TiO_2 sol, the PS microspheres were removed by sonication in toluene, and the nanoporous TiO_2 ring template was obtained. (e) A low temperature hydrothermal method was used to achieve the patterned and aligned growth of ZnO nanorod arrays on the patterned GaN substrate.

The size of template depends on the diameter of the initial PS microspheres. However, the size of PS microspheres commercially available is limited, and it becomes increasingly difficult to keep the hexagonal close-packing order of PS microspheres with diameters below 200 nm. Actually, most reports on NSL technology deal with colloidal spheres with diameters of 300 nm and larger. An alternative approach is to start with SAM of PS microspheres with an appropriate diameter, and then etch them to the desirable size. Anisotropic RIE were used to etch the PS microspheres whose dimension can be easily controlled by adjusting the etching time and conditions.[22−24] Figure 2 shows the SEM images of the PS microspheres suffered oxygen RIE for different time intervals. Since the etching rate of the GaN substrate is much smaller than that of the PS microsphere, the substrate remained almost unetched. During this process, the morphology of SAM has turned to nonclose-packed (ncp) monolayer, while inheriting the long-range hexagonal order. For the anisotropic RIE, the reaction occurs in a reactive ion plasma etching chamber, with a unidirectional electric field to guide the direction of the reaction.[25] As a result, the PS microspheres transferred to oblate ellipsoids, as shown in Figure 2f. Furthermore, long time RIE etching yields a rather rough surface, which is desirable for tailoring the wetting behavior of PS microsphere surface to guarantee the coating of TiO_2 sol. By varying the time of oxygen RIE, we can obtain the ncp monolayers of PS microspheres with different sizes. Figure 2b-e give the SEM images of the PS microsphere SAM exposing to the anisotropic oxygen plasma for 1, 1.5, 2, and 2.5 min, respectively, and the corresponding diameters of these samples are 420, 370, 310, and 140 nm. Additionally, etching time dependence of the diameter of PS microspheres (see Figure S1 in the Supporting

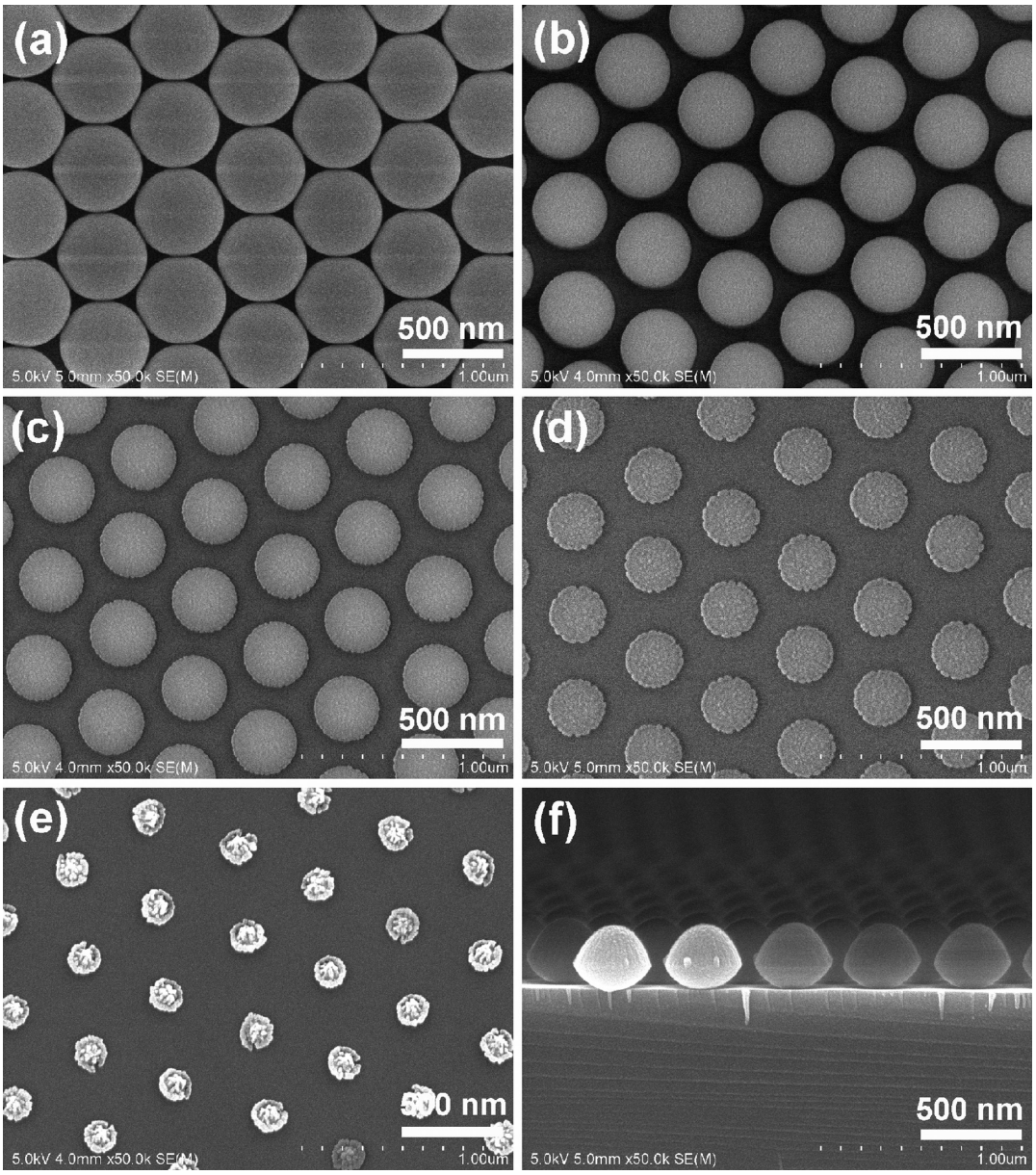

Figure 2. SEM images of (a) the initial 500 nm PS microspheres in closely packed arrays, nonclose-packed PS microspheres by anisotropic oxygen RIE for (b) 1 min, (c) 1.5 min, (d) 2 min, and (e) 2.5 min; (f) side view of PS microspheres etched for 1.5 min.

Information) indicates a highly nonlinear behavior, as reported previously for RIE of colloids.[22,23] In marked contrast, a linear relationship has been observed for isotropic etching, because of the constant radial etching rate during the whole process.[26]

We also tried the isotropic plasma etching of the PS microspheres. As shown in Figure S2 in the Supporting Information, by exposing the PS microsphere SAM to the isotropic O-plasma for a certain time interval, the diameter of PS microspheres is clearly reduced, while conserving the perfect spherical shape. However, most of the PS microspheres shift their positions and the long-range hexagonal order is destroyed. The similar phenomenon has been observed and interpreted by Plettl et al.[26] This position-shift can be avoided by etching at a low temperature of −150 °C, but the cost will be raised hugely in that case. Considering the perfect spherical shape is not essential in our experiments, the anisotropic RIE was adopted in this work.

To generate the inverted SAM mask, the TiO_2 sol was prepared and applied on the GaN substrate coated with the PS microsphere monolayer by spin-coating. After solidification of the TiO_2 sol, the PS microspheres were selectively and completely removed by sonication in toluene. Figure 3 shows the AFM images of TiO_2 ring templates by using the PS microspheres with different sizes. Obviously, the long-range hexagonal order inheriting from the initial SAM template is conserved. The inner diameter of TiO_2 ring decreases significantly from around 400 to 50 nm, when the diameter of PS microsphere is reduced from 500 to 140 nm by oxygen plasma exposure for increasing time intervals. As the latex solution of PS microsphere is applied and dried on the GaN substrate, the deformability of the PS microspheres results in the plane contact between them and the substrate. The decrease of the contact area with the size of PS microsphere leads to the reduction of the inner diameter of TiO_2 ring.

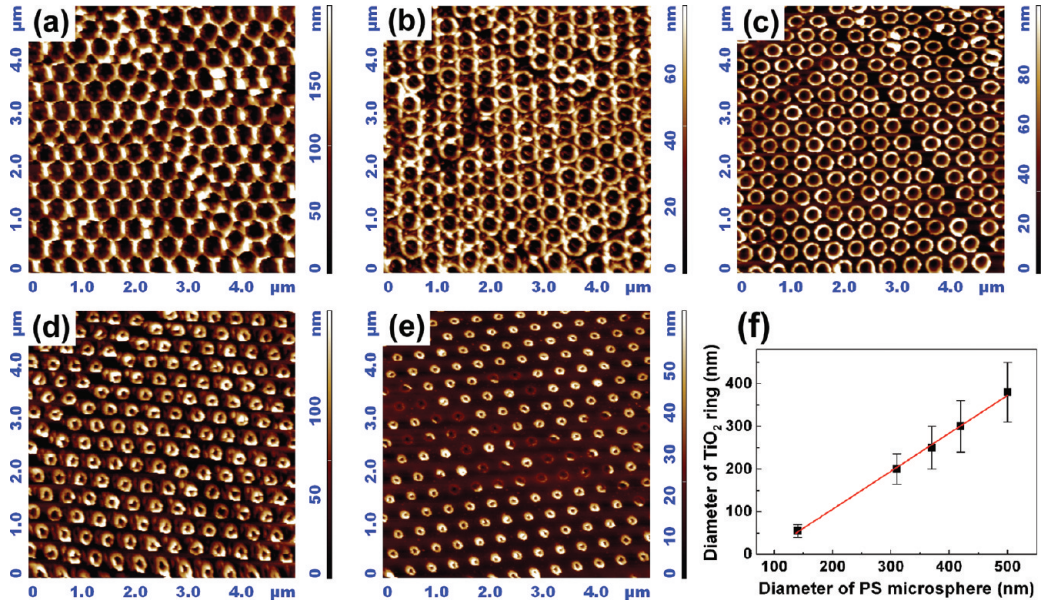

Figure 3. AFM topographies of TiO_2 ring templates by using (a) the initial 500 nm PS microspheres; and the PS microspheres etched for (b) 1.0, (c) 1.5, (d) 2.0 and (e) 2.5 min. (f) The influence of the size of PS microspheres on the inner diameter of TiO_2 ring templates.

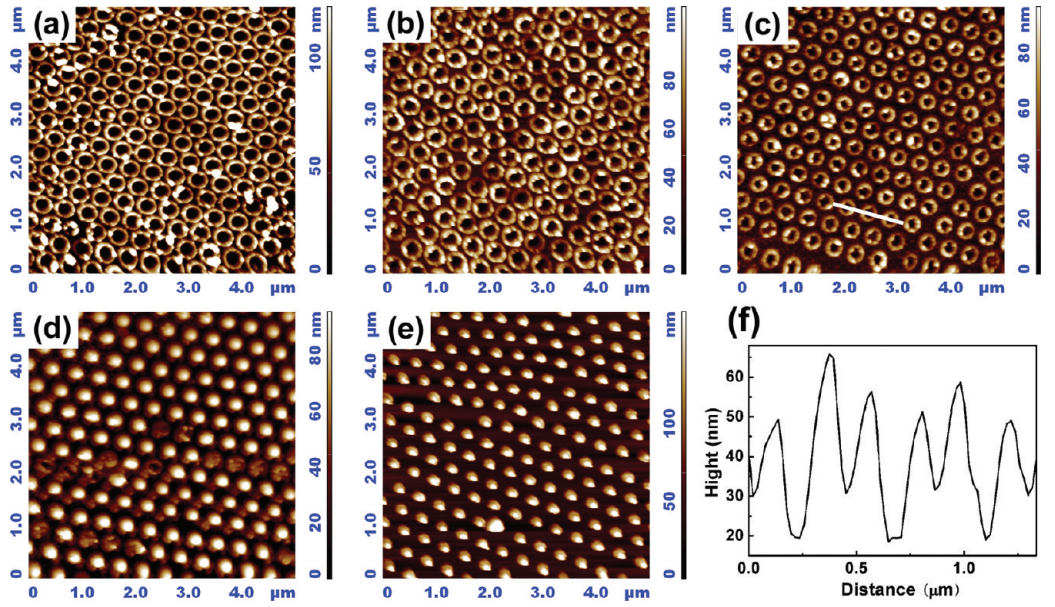

Figure 4. AFM topographies of TiO_2 ring templates created by spin-coating of TiO_2 sol with the concentrations of (a) 0.04, (b) 0.06, (c) 0.12 and (d) 0.24 M on the 370 nm PS microspheres (etched for 1.5 min). (e) The TiO_2 ring template prepared by using the 140 nm PS microspheres (etched for 2.5 min) and the TiO_2 sol with the concentrations of 0.06 M. (f) The height profile along the cursor line in Figure 4c.

On the other hand, the concentration of TiO_2 sol plays a role in fine-tuning the diameter of TiO_2 ring. As presented in Figure 4a-c, when the concentration is 0.04, 0.06, and 0.12 M for the 370 nm PS microspheres (etched for 1.5 min), the corresponding inner diameter of TiO_2 rings is around 300, 250, and 200 nm, respectively. Further increasing the concentration of TiO_2 sol up to 0.24 M, the PS microspheres are closely covered with TiO_2 sol and can not be removed anymore (Figure 4d). As soon as being applied on the PS microsphere SAM, the TiO_2 sol will surround the PS microspheres as a result of the capillary force produced by the wedge areas between the PS microspheres and the substrate.[27] TiO_2 sol with a higher concentration introduces more solute, and much worse fluidity on the substrate, so the inner diameter of TiO_2 rings gets smaller and the ring-wall grows thicker. As the concentration goes beyond a certain value, the PS microspheres will be closely packed. Obviously, smaller in size of PS microspheres, it is easier to be closely covered with TiO_2 sol, thus the closely packed concentration decreases with the size of PS microsphere. For example, the closely covered concentration is as low as 0.06 M (Figure 4e) for the PS microspheres etched for 2.5 min (140 nm in diameter). Consequently, to obtain the TiO_2 ring arrays, the

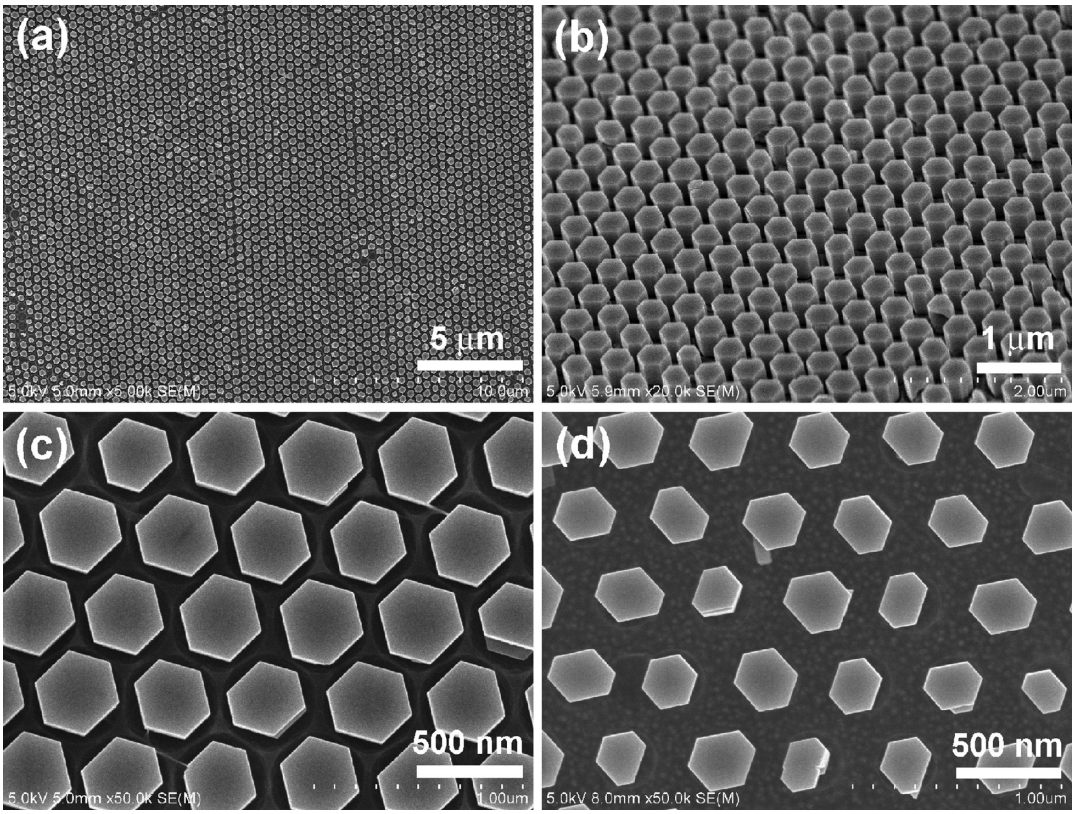

Figure 5. (a, c, d) Top view and (b) 45° tilt view of the patterned and aligned ZnO nanorod arrays on the GaN substrate grown by hydrothermal reaction. The TiO_2 ring templates used for these ZnO nanorod arrays were prepared (a-c) with the initial 500 nm PS microspheres, and (d) with the 370 nm PS microspheres (etched for 1.5 min).

concentration of TiO_2 sol should be confined in a certain range to avoid closely packing. Figure 3f summarizes the influence of both the size of PS microsphere and the concentration of TiO_2 sol on the inner diameter of TiO_2 ring arrays. It can be seen that the inner diameter of TiO_2 rings, with a smaller value compared with the corresponding PS microspheres, varies linearly with the diameter of PS microspheres, while the concentration of TiO_2 sol plays the role of fine-tuning, as shown by error bar in Figure 3f. Above all, taking advantage of RIE and the TiO_2 sol with different concentrations, we can adjust the diameter of TiO_2 rings potentially from about 40 to 450 nm for the 500 nm PS microsphere. In addition, from the height profile (see Figure 4f) of the line drawn in Figure 4c, it can be seen that the area outside the rings is about ten nanometers higher than the inside uncovered substrate, implying that the interstitial area of the TiO_2 rings is covered by a ~10 nm TiO_2 film. Therefore, there is a circular area of bare GaN substrate inside each TiO_2 ring, which can serve as the active site for the site-specific growth of ZnO nanorods during the hydrothermal process.

Patterned and aligned ZnO nanorod arrays on the GaN substrates were grown in aqueous solution containing 0.05 M $Zn(NO_3)_2 \cdot 6H_2O$ and HMTA at 50 °C for 6 h. Figure 5 shows the top and 45° tilt view of the as-grown ZnO nanorods with uniform diameter and height. It can be seen that the nanorod arrays reserve the long-range hexagonal periodicity of the original PS microsphere SAM, and the spacing between two neighboring nanorods is 500 nm which is predefined by the PS template. All of the nanorods are perfectly aligned normal to the substrate and a defect-less region can be achieved at least on the scale of $20 \times 20\ \mu m^2$. A few point defects are observed in some areas which can be attributed to the defects in the original PS microsphere SAM. From Figure 5c, we can see that all the nanorods are hexagonal-faceted with very smooth surface as well as uniform diameter of 380 nm close to the inner diameter of TiO_2 rings in use, and only single nanorod is grown at each growth site. The hexagonal faces of ZnO nanorods indicate that each nanorod is a single crystal of wurtzite ZnO with growth direction along [0001]. Besides, the hexagonal nanorods are well oriented with their side faces parallel to each other, indicating the perfect epitaxial growth of ZnO nanorods on the GaN substrate.

The size-control of ZnO nanorod arrays is realized by changing the inner diameter of TiO_2 rings. Two TiO_2 ring templates with the inner diameters of 380 nm (unetched PS microsphere) and 200 nm (etched for 1.5 min) were adopted. Hydrothermal growths at the same conditions were performed and the corresponding results were shown in Figure 5c, d. For both samples, the spacing between two neighboring nanorods remains 500 nm as determined by the size of PS microspheres, while the diameters of ZnO nanorods, 380 and 220 nm, are closely related to the inner diameters of underlying TiO_2 ring templates. The slightly increase in the diameter is due to the lateral growth of ZnO nanorods. Combined with the adjustment of the TiO_2 ring template shown in Figures 3 and 4, the diameter of the individual ZnO nanorod can be potentially tuned over a wide range.

To investigate the growth process of ZnO nanorod arrays, hydrothermal growths at different solution concentrations and reaction temperatures were also performed. As shown in Figure 6a, b, the patterned array of ZnO nanorod bundles, rather than single

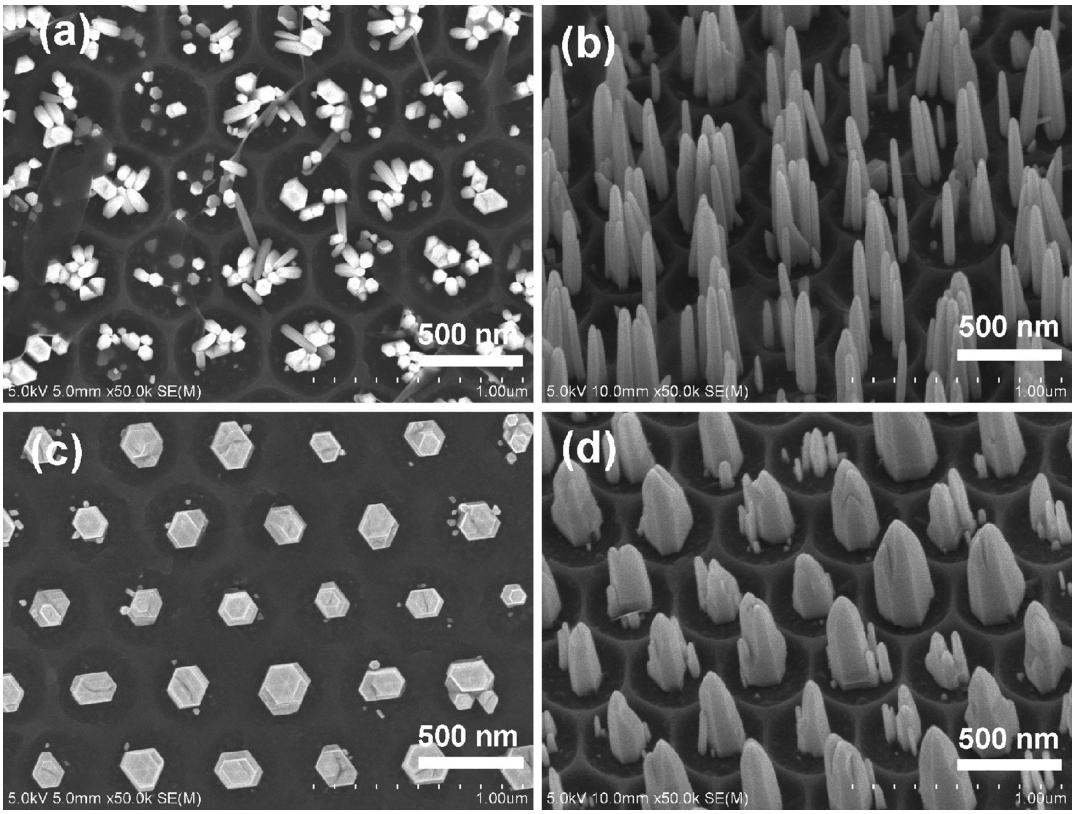

Figure 6. Patterned ZnO nanorod arrays on the GaN substrate grown at different solution concentrations and reaction temperatures, (a, b) 0.02 M, 50 °C for 6 h, (c, d) 0.02 M, 90 °C for 2 h.

nanorod from each growth site, was obtained at lower solution concentration of 0.02 M and reaction temperature of 50 °C. In this case, multinuclei have formed at one single growth site at the beginning of growth process, which guides the subsequent growth of ZnO nanorods, resulting in multiple ZnO nanorods. By increasing the temperature to a higher value of 95 °C, while keeping the concentration at 0.02 M, those ZnO nanorod bundles were inclined to convert to the individual nanorod array. However, the conversion of these nanorod bundles was not complete, consequently, the individual nanorod was only achieved at a part of these growth sites, as shown in Figure 6c, d. It is possible that multinuclei formed at each growth site because of the low solution concentration, during the growth process those multiple ZnO nanorods merged into a thicker nanorod under appropriate conditions. When the solution concentration increased to 0.05 M, the individual nanorod was grown from each growth site even though at a lower reaction temperature of 50 °C, as shown in Figure 5a-c. Both higher solution concentration and reaction temperature may favor the individual growth model of ZnO nanorods due to the faster feeding of the reactant ions to the growth sites. The similar phenomenon has been observed in previous reports,[13,18] in which they proposed that the mergence of multiple ZnO nanorods to individual nanorod could be attributed to the coalescence effects of ZnO nanorods in close proximity. Our results indicate that the solution concentration plays a more important role than the reaction temperature to realize the individual growth.

The XRD spectrum of the patterned ZnO nanorod array is presented in Figure 7a, with each Bragg peak having assigned its identification and Millar indices. From the zoom-in view (lower inset of Figure 7a), one can see that ZnO (0002) and GaN (0002) peaks are separated clearly and located at 34.44° and 34.58°, respectively. Besides, three peaks are clearly observed at 41.70°, 72.56° and 72.88°, corresponding to Al_2O_3 (0006), ZnO (0004) and GaN (0004), respectively. The absence of any other peaks from ZnO, within the experimental resolution, indicates the high *c*-axis orientation of the as-grown ZnO nanorod array. To judge the epitaxial quality of the ZnO nanorod array, the rocking curve of the ZnO (0002) reflection was recorded (upper inset of Figure 7a), which is rarely given for the patterned ZnO nanostructures. It exhibits a full width at half-maximum (fwhm) value of 0.2°, indicating high epitaxial quality and perfect vertical alignment of the ZnO nanorod array on the GaN substrate. Recently, Xu et al.[13] present the rocking curve of the ZnO (0002) peak with a smaller fwhm value of 0.15°, in which the patterned ZnO nanowire arrays were prepared by the combination of hydrothermal method and EBL. However, besides ZnO (0002) and (0004) peaks, the ZnO (110) peak was observed clearly in their θ-2θ scanning results, implying an unperfect *c*-axis orientation. Moreover, the NSL technique adopted in our work is much more accessible and economical than the EBL.

To further analyze the in-plane orientation of ZnO nanorod arrays, phi-scans were taken on the $\{10-11\}$ planes of both the ZnO nanorod array and the GaN substrate. As shown in Figure 7b, the phi-scan of $\{10-11\}$ exhibits six sharp peaks at 60° intervals, revealing the expected 6-fold rotational symmetry about the ZnO $[0001]$ direction, which agrees with the previous SEM images. It is worth noting that the azimuthal angular spread for the ZnO nanorod array is considerably narrow (0.35°), which has never been reported for patterned ZnO nanorod arrays

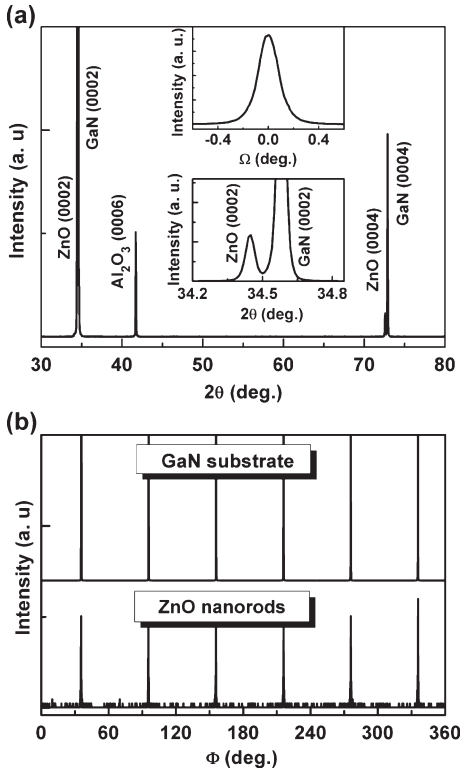

Figure 7. (a) XRD pattern of the as-grown ZnO nanorod arrays in a normal θ-2θ configuration. The lower inset is the zoom-in view of ZnO (0002) and GaN (0002), and the upper inset is the rocking curve for the ZnO (0002) peak. (b) The phi-scan on the {10−11} plane of both the ZnO nanorod array and the GaN substrate.

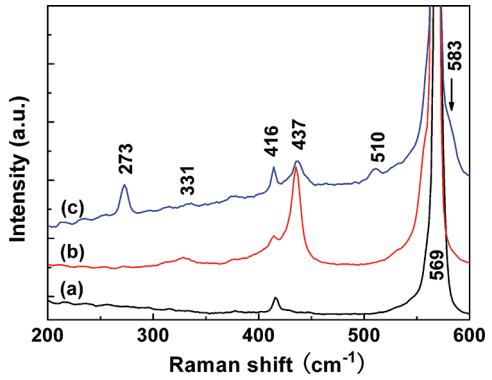

Figure 8. Raman spectra of (a) the GaN/sapphire substrate, (b) the as-grown ZnO nanorod array, and (c) the ZnO thin film measured at room temperature.

previously, indicating an excellent in-plane orientation. Furthermore, the peaks in the phi-scan of GaN {10−11} have the same symmetry and were detected at essentially identical values of the in-plane rotation angle, indicating the epitaxial growth of the ZnO nanorod array on the GaN substrate. Based on the XRD results, the epitaxial relationship between the ZnO nanorods and the GaN substrate is determined to be: ZnO (0002)[10−10]‖ GaN (0002)[10−10].

The high crystallinity of the patterned ZnO nanorod arrays was also confirmed by Raman scattering measurements that presented information on the vibrational properties of materials. Figure 8 shows the Raman spectrum of the as-grown ZnO nanorod array. For comparison, the Raman spectra of the GaN/sapphire substrate and the ZnO thin film prepared by magnetron sputtering are also included in Figure 8. Two Raman peaks at 416 and 569 cm^{-1}, which are observed from all the samples, are attributed to sapphire and GaN, respectively. In addition to the Raman peaks originating from the substrate, there are two peaks at 437 and 331 cm^{-1} shared by both Raman spectra of the ZnO nanorod array and the ZnO thin film. The strong peak at 437 cm^{-1} can be assigned to E_2(high) mode of ZnO, corresponding to the characteristic band of the hexagonal wurtzite structure, whereas the weaker peak at 331 cm^{-1} belongs to the E_2(high)-E_2(low) mode of ZnO.[28] The most important feature, however, of the results presented in this figure, is the fact that three peaks at 273, 510, and 583 cm^{-1} are only observed from the Raman spectrum of the ZnO thin film. These peaks belong to neither first- nor second- order structures of ZnO, and usually are called as anomalous Raman peaks. According to the previous reports,[29−31] some silent Raman modes can be activated by disorder in the crystal because of the relaxation of the Raman selection rules produced by the breakdown of the translational symmetry of the crystal lattice. These anomalous peaks at 273, 510, and 583 cm^{-1} can be assigned to B_1(low), $2B_1$(low) and E_1(LO) silent modes, respectively, which are activated by lattice defects in ZnO.[29−31] Therefore, the absence of the anomalous Raman peaks demonstrates that the patterned ZnO nanorod array is of high crystalline quality. Furthermore, the photoluminescence (PL) spectrum of the as-grown ZnO nanorod array presents a unique ultraviolet (UV) emission (to be reported elsewhere), while the defect related visible emission can not be observed, implying the high crystal quality of the ZnO nanorods on GaN.

4. CONCLUSION

In summary, we have developed an effective approach to the controllable growth of highly ordered and vertically aligned ZnO nanorod arrays on the GaN substrate via a hydrothermal route by using the TiO_2 ring template deriving from the PS microsphere SAM. Taking advantage of the oxygen RIE on PS microspheres, the dimension of TiO_2 rings can be flexibly adjusted ranging from 50 to 400 nm. As a result, the diameter of the individual ZnO nanorods can be potentially tuned over a wide range. The ordered ZnO nanorods are highly uniform in diameter and height with perfect alignment and are epitaxially grown along [0001] direction. The absence of the anomalous Raman peaks demonstrates that the patterned ZnO nanorod array is of high crystalline quality. The excellent properties of these ZnO nanorod arrays promise their potential applications in advanced photonic optical devices.

■ ASSOCIATED CONTENT

Supporting Information. Etching time dependence of the diameter of PS microspheres by RIE; the SEM images of the PS microspheres SAM suffered isotropic plasma etching. This material is available free of charge via the Internet at http://pubs.acs.org.

■ AUTHOR INFORMATION

Corresponding Author

*Corresponding author. E-mail: xwzhang@semi.ac.cn.

■ ACKNOWLEDGMENT

This work was financially supported by the "863" project of China (Grant No. 2009AA03Z305), the National Natural Science Foundation of China (Grant No. 60876031, 51071145) and the National Basic Research Program of China (Grant No. 2012CB934200).

■ REFERENCES

(1) Lee, S. W.; Jeong, M. C.; Myoung, J. M. *Appl. Phys. Lett.* **2007**, *90*, 133115.
(2) Wang, X. D.; Song, J. H.; Liu, J.; Wang, Z. L. *Science* **2007**, *316*, 102–105.
(3) Lee, Y. J.; Ruby, D. S.; Peters, D. W.; McKenzie, B. B.; Hsu, J. W. P. *Nano Lett.* **2008**, *8*, 1501–1505.
(4) Matsuu, M.; Shimada, S.; Masuya, K.; Hirano, S.; Kuwabara, M. *Adv. Mater.* **2006**, *18*, 1617–1621.
(5) Kim, K. S.; Jeong, H.; Jeong, M. S.; Jung, G. Y. *Adv. Funct. Mater.* **2010**, *20*, 3055–3063.
(6) Djurisic, A. B.; Leung, Y. H. *Small* **2006**, *2*, 944–961.
(7) Xu, S.; Xu, C.; Liu, Y.; Hu, Y. F.; Yang, R. S.; Yang, Q.; Ryou, J.; Kim, H. J.; Lochner, Z.; Choi, S.; Dupuis, R.; Wang, Z. L. *Adv. Mater.* **2010**, *22*, 4749–4753.
(8) Ng, H. T.; Han, J.; Yamada, T.; Nguyen, P.; Chen, Y. P.; Meyyappan, M. *Nano Lett.* **2004**, *4*, 1247–1252.
(9) Kim, D. S.; Ji, R.; Fan, H. J.; Bertram, F.; Scholz, R.; Dadgar, A.; Nielsch, K.; Krost, A.; Christen, J.; Gösele, U.; Zacharias, M. *Small* **2007**, *3*, 76–80.
(10) Martensson, T.; Carlberg, P.; Borgström, M.; Montelius, L.; Seifert, W.; Samuelson, L. *Nano Lett.* **2004**, *4*, 699–702.
(11) Hochbaum, A. I.; Fan, R.; He, R.; Yang, P. *Nano Lett.* **2005**, *5*, 457–460.
(12) Greene, L. E.; Law, M.; Goldberger, J.; Kim, F.; Johnson, J. C.; Zhang, Y. F.; Saykally, R. J.; Yang, P. D. *Angew. Chem., Int. Ed.* **2003**, *42*, 3031–3034.
(13) Xu, S.; Wei, Y. G.; Kirkham, M.; Liu, J.; Mai, W. J.; Davidovic, D.; Snyder, R. L.; Wang, Z. L. *J. Am. Chem. Soc.* **2008**, *130*, 14958–14959.
(14) Yuan, D.; Guo, R.; Wei, Y. G.; Wu, W. Z.; Ding, Y.; Wang, Z. L.; Das, S. *Adv. Funct. Mater.* **2010**, *20*, 3484–3489.
(15) Liu, N. S.; Fang, G. J.; Zeng, W.; Long, H.; Yuan, L. Y.; Zhao, X. Z. *Appl. Phys. Lett.* **2009**, *95*, 153505.
(16) Rybczynski, J.; Banerjee, D.; Kosiorek, A.; Giersig, M.; Ren, Z. F. *Nano Lett.* **2004**, *4*, 2037–2040.
(17) Liu, D. F.; Xiang, Y. J.; Wu, X. C.; Zhang, Z. X.; Liu, L. F.; Song, L.; Zhao, X. W.; Luo, S. D.; Ma, W. J.; Shen, J.; Zhou, W. Y.; Wang, G.; Wang, C. Y.; Xie, S. S. *Nano Lett.* **2006**, *6*, 2375–2378.
(18) Li, C.; Hong, G. S.; Wang, P. W.; Yu, D. P.; Qi, L. M. *Chem. Mater.* **2009**, *21*, 891–897.
(19) Zeng, H. B.; Xu, X. J.; Bando, Y.; Gautam, U. K.; Zhai, T. Y.; Fang, X. S.; Liu, B. D.; Golberg, D. *Adv. Funct. Mater.* **2009**, *19*, 3165–3172.
(20) Cheng, C.; Lei, M.; Feng, L.; Wong, T. L.; Ho, K. M.; Fung, K. K.; Loy, M. M. T.; Yu, D. P.; Wang, N. *ACS Nano* **2009**, *3*, 53–58.
(21) Park, S. H.; Roy, A.; Beaupré, S.; Cho, S.; Coates, N.; Moon, J. S.; Moses, D.; Leclerc, M.; Lee, K.; Heeger, A. *Nat. Photonics* **2009**, *3*, 297–302.
(22) Haginoya, C.; Ishibashi, M.; Koike, K. *Appl. Phys. Lett.* **1997**, *71*, 2934–2936.
(23) Yan, L. L.; Wang, K.; Wu, J. S.; Ye, L. *J. Phys. Chem. B* **2006**, *110*, 11241–11246.
(24) Huang, Z.; Fang, H.; Zhu, J. *Adv. Mater.* **2007**, *19*, 744–748.
(25) Deng, T.; Cournoyer, J. R.; Schermerhorn, J. H.; Balch, J.; Du, Y.; Blohm, M. L. *J. Am. Chem. Soc.* **2008**, *130*, 14396–14397.
(26) Plettl, A.; Enderle, F.; Saitner, M.; Manzke, A.; Pfahler, C.; Wiedemann, S.; Ziemann, P. *Adv. Funct. Mater.* **2009**, *19*, 3279–3284.
(27) Sun, F. Q.; Yu, J. C.; Wang, X. C. *Chem. Mater.* **2006**, *18*, 3774–3779.
(28) Cuscó, R.; Alarcón-Lladó, E.; Ibáñez, J.; Artús, L.; Jiménez, J.; Wang, B.; Callahan, M. J. *Phys. Rev. B* **2007**, *75*, 165202.
(29) Dong, J. J.; Zhang, X. W.; You, J. B.; Cai, P. F.; Yin, Z. G.; An, Q.; Ma, X. B.; Jin, P.; Wang, Z. G.; Chu, P. K. *ACS Appl. Mater. Interfaces* **2010**, *2*, 1780–1784.
(30) Manjón, F. J.; Marí, B.; Serrano, J.; Romero, A. H. *J. Appl. Phys.* **2005**, *97*, 053516.
(31) Bundesmann, C.; Ashkenov, N.; Schubert, M.; Spemann, D.; Butz, T.; Kaidashev, E. M.; Lorenz, M.; Grundmann, M. *Appl. Phys. Lett.* **2003**, *83*, 1974–1976.